Ultrasound in Med. & Biol., Vol. 34, No. 11, pp. 1808–1819, 2008

0301-5629/08/$–see front matter

ELSEVIER

doi:10.1016/j.ultrasmedbio.2008.04.011

● *Original Contribution*

HYBRID SPECTRAL DOMAIN METHOD FOR ATTENUATION SLOPE ESTIMATION

HYUNGSUK KIM and TOMY VARGHESE
Department of Medical Physics, Department of Electrical and Computer Engineering, The University of Wisconsin-Madison, Madison, WI, USA

(*Received* 12 *June* 2007; *revised* 27 *March* 2008; *in final form* 18 *April* 2008)

Abtract—Attenuation estimation methods for medical ultrasound are important because attenuation properties of soft tissue can be used to distinguish between benign and malignant tumors and to detect diffuse disease. The classical spectral shift method and the spectral difference method are the most commonly used methods for the estimation of the attenuation; however, they both have specific limitations. Classical spectral shift approaches for estimating ultrasonic attenuation are more sensitive to local spectral noise artifacts and have difficulty in compensating for diffraction effects because of beam focusing. Spectral difference approaches, on the other hand, fail to accurately estimate attenuation coefficient values at tissue boundaries that also possess variations in the backscatter. In this paper, we propose a hybrid attenuation estimation method that combines the advantages of the spectral difference and spectral shift methods to overcome their specific limitations. The proposed hybrid method initially uses the spectral difference approach to reduce the impact of system-dependent parameters including diffraction effects. The normalized power spectrum that includes variations because of backscatter changes is then filtered using a Gaussian filter centered at the transmit center frequency of the system. A spectral shift method, namely the spectral cross-correlation algorithm is then used to compute spectral shifts from these filtered power spectra to estimate the attenuation coefficient. Ultrasound simulation results demonstrate that the estimation accuracy of the hybrid method is better than the centroid downshift method (spectral shift method), in uniformly attenuating regions. In addition, this method is also stable at boundaries with variations in the backscatter when compared with the reference phantom method (spectral difference method). Experimental results using tissue-mimicking phantom also illustrate that the hybrid method is more robust and provides accurate attenuation estimates in both uniformly attenuating regions and across boundaries with backscatter variations. The proposed hybrid method preserves the advantages of both the spectral shift and spectral difference approaches while eliminating the disadvantages associated with each of these methods, thereby improving the accuracy and robustness of the attenuation estimation. (E-mail: hyungsukkim@wisc.edu) **© 2008 World Federation for Ultrasound in Medicine & Biology.**

Key Words: **Attenuation, Attenuation coefficient, Parametric imaging, Power spectrum, Spectral shift, Spectral difference, Tissue characterization, Ultrasound.**

INTRODUCTION

Ultrasound pulse–echo systems have been used widely for imaging large solid organs in the human body, as well as for evaluating the pathologic state of tissue. Various tissue parameters including speed of sound (Robinson et al. 1991; Techavipoo et al. 2004; Levy et al. 2006), integrated backscatter (Vered et al. 1989; Wear et al. 2005; Bridal et al. 2006; Taggart et al. 2007) and scatterer size (Insana and Wagner 1990; Hall et al. 1996; Liu et al. 2006) are extracted by quantitative analysis of radiofrequency (RF) data. Ultrasound attenuation is also one of critical parameters of soft tissue used to distinguish malignant from benign tumors and detect diffuse diseases in liver (Narayana and Ophir 1983; Fujii et al. 2002; Meziri et al. 2005), breast (Huang and Li 2005), bone (Wear 2001, 2003), intercostal tissue (Towa et al. 2002) and the myocardium (Baldwin et al. 2006).

Many different algorithms have been studied to estimate ultrasound attenuation in the literature. These methods can be classified as either time–domain or frequency–domain approaches. In the time domain, He and Greenleaf (1986) used the variations of the local maximum along the echo signal envelope to estimate the attenuation coefficient. Jang et al. (1998) proposed to

Address correspondence to: Hyungsuk Kim, Department of Electrical and Computer Engineering, The University of Wisconsin-Madison, Madison, WI 53706. E-mail: hyungsukkim@wisc.edu

estimate this parameter by measuring the difference in entropy between adjacent narrowband echo signals. A method based on the analysis of video or B-scan images has also been proposed by Knipp et al. (1997). In general, time–domain approaches are easier to implement and computationally faster than frequency–domain approaches. However, local variations in the sound field (diffraction effects) as the beam propagates are very difficult to compensate in the time domain. Therefore, many frequency–domain algorithms have been studied to estimate attenuation properties.

In the frequency domain, there are two fundamental types of methods to estimate the attenuation coefficient, namely spectral difference and spectral shift methods. Spectral difference methods calculate the amplitude decay of the power spectra from the backscattered RF signals (Yao et al. 1990), while spectral shift methods calculate the downshift of the center frequency of the power spectrum calculated at different depths (Kuc and Li 1985). The amplitude decay along the beam propagation direction using narrowband pulses (Ophir et al. 1985) and the amplitude changes in the time–frequency representation (Zhao et al. 2004) have been used to estimate attenuation. Yao et al. (1990) developed a method to reduce system and transducer dependencies, including the effects of diffraction, using a reference phantom of which the attenuation parameters are known *a priori*. However, with spectral difference methods, problems occur at boundaries between two regions of different backscatter properties, because the amplitude of the power spectra depends also on these backscatter properties. For the spectral shift approaches, Fink et al. (1983) developed the centroid downshift method using short-time Fourier analysis techniques. The phase lag in the autocorrelation function of the complex echo signals (Kasai et al. 1985) and second-order autoregressive models (Kuc and Li 1985; Baldeweck et al. 1995) have also been used to estimate the center frequency shift in the power spectrum. Although spectral shift methods are more robust than spectral difference methods for estimation of the attenuation coefficient at boundaries with backscatter changes, they are more sensitive to local spectral noise artifacts and have difficulty in compensating for diffraction effects.

Besides the development of various estimation algorithms in both frequency and time domain, the estimation accuracy in terms of spatial resolution (or block size) is another important aspect for attenuation imaging. Zagzebski et al. (1993) found that the minimum size of the gated window along the axial direction should be at least 4 μs in liver tissue to obtain reliable estimation results in the frequency domain. The estimation accuracy for different window sizes was compared using Gaussian transformation and spectral fit algorithms (Bigelow et al. 2005). Bigelow et al. (2005) reported reasonable estimation accuracy using a 4-mm data segment gated with a Hamming window for attenuation values between 0.05 and 1 dB/cm/MHz when 25 waveforms per gated window, whose frequency bandwidth is 4–11 MHz, were used. In the time domain, Baldwin et al. (2005) evaluated the estimation accuracy and precision of attenuation estimated for various gated window sizes on myocardial tissue using an image-based estimation technique. They reported that significant estimation differences were observed for window sizes smaller than 4 mm using a linear array with a frequency bandwidth of 4–7 MHz and a center frequency of 5.5 MHz. Because the scattering properties can vary across tissue and change with the wavelength of the insonifying pulse, the optimum block size may differ based on tissue type and insonification frequency. Therefore, the stability of the power spectra obtained with different block sizes have to be evaluated before the estimation of the attenuation parameters. For attenuation estimation, we presented a criterion based on the full-width-half-maximum (FWHM) value of the power spectra (Kim and Varghese 2007). The optimal block size for the RF data is selected as the minimum window size required to obtain a stable FWHM value. In general, if the gated window is too short, spectral broadening of the power spectra is observed, which can introduce errors in the estimation of the attenuation.

In this paper, we propose a hybrid method of estimation of the attenuation in the frequency domain, which exploits the advantages of both the spectral difference algorithm and the spectral shift algorithm to overcome their respective limitations. In a first step, this hybrid method uses the reference phantom method to normalize the power spectra obtained at different depths (Yao et al. 1990), as it is done in the traditional spectral difference algorithm. This normalization process eliminates transfer functions associated with the ultrasound system, diffraction effects and the transmitted pulse. The transfer function of the transmitted pulse is then reintroduced by filtering the normalized power spectrum using a Gaussian filter centered on the transmit center frequency of the system. The resulting filtered power spectra are still affected by the potential differences in backscatter between different regions. Therefore, in a second step, a spectral shift method based on the spectral cross-correlation algorithm (Kim and Vargheses 2007) is used to estimate, from these filtered spectra, the attenuation coefficient.

In this paper, a theoretical derivation of the hybrid algorithm will be presented. This new algorithm for the estimation of the attenuation will be compared with the traditional spectral shift and spectral difference methods, using both simulated and experimental RF data. Finally,

our results will be discussed and conclusions about the proposed method presented.

MATERIALS AND METHODS

Hybrid spectral domain algorithm

Most methods that estimate the attenuation coefficient using pulse–echo data assume linear frequency dependence of the attenuation, uniform backscatter and constant speed-of-sound in the region-of-interest (ROI). Other assumptions include weak scattering in tissue, which allows for multiple scattering to be ignored (Born approximation). Under these assumptions, the intensity of the backscattered RF signal received at the ultrasound transducer $S(f,z)$ can be expressed in the frequency domain as a product of the transmit pulse, diffraction effects, attenuation effects and backscatter terms, which is defined as

$$S(f,z) = P(f)\cdot D(f,z)\cdot A(f,z)\cdot B(f), \tag{1}$$

where z denotes the depth of the ROI from the transducer, $P(f)$ represents the combined effect of the transmit pulse and transducer sensitivity (electroacoustic and acoustoelectric transfer functions), which depends on the transducer design and the transmit pulse. $D(f,z)$ denotes the effect of diffraction related to the geometry of the transducer, and $A(f,z)$ represents the cumulative attenuation in soft tissue. In a medium with uniform attenuation property, the cumulative attenuation can be expressed as

$$A(f,z) = \exp\{-4\alpha(f)\,z\}, \tag{2}$$

where $\alpha(f)$ is the coefficient of attenuation expressed in Np/cm (or dB/cm). $\alpha(f)$ is commonly assumed to be linearly proportional to the frequency (Flax et al. 1983; Kuc 1985) and therefore can be written as $\alpha(f) = \beta\cdot f$, where β is the slope of the attenuation expressed in Np/cm/MHz (or dB/cm/MHz).

The backscattered echo signals denoted by $B(f)$ in eqn (1) are modeled as a power of frequency and expressed in an exponential form of the Taylor series expansion, which is then used to derive a closed-form expression for the spectral shift in the frequency domain (Berger et al. 1990; Treece et al. 2005):

$$\begin{aligned} B(f) = f^n &= \exp\{n\cdot\log(f)\} \\ &= \exp\left\{n\cdot\log(f_c) + n\cdot\log\left(1+\frac{f-f_c}{f_c}\right)\right\} \\ &\approx f_c^{\,n}\cdot\exp\left\{n\cdot\left(\frac{f-f_c}{f_c} - \frac{(f-f_c)^2}{2f_c^{\,2}}\right)\right\} \\ &\propto \exp\left\{-\frac{n\cdot(f^2-4f_cf)}{2f_c^{\,2}}\right\}, \end{aligned} \tag{3}$$

where f_c is the center frequency of a transmit pulse. The expression shown in eqn (3) ignores higher-order terms of the Taylor's series expansion. Any terms that are not a function of the frequency in eqn (3) can be ignored because they do not affect the estimation of the centroid in the spectral shift estimation method. The parameter n can vary from 0 for specular scattering to 4 for Rayleigh scattering. Typical values of n for human tissue are between 1 and 2 (Wear et al. 1995).

The ratio of the intensity of the backscattered RF signals from the sample to that from a reference phantom recorded using identical transducer and system settings have been used previously to eliminate transducer-dependent terms, *i.e.*, $P(f)$ and $D(f,z)$. Thus, the ratio of the intensities of the echo signals at depth z from a sample to that from a reference phantom at the same depth in uniform backscatter region is expressed as (Yao et al. 1990)

$$\begin{aligned} RS(f,z) &= \frac{B_s(f)}{B_r(f)}\cdot\exp\{-4\,(\beta_s-\beta_r)\,f\,z\} \\ &= \exp\left\{-\frac{(n_s-n_r)\cdot(f^2-4f_cf)}{2f_c^{\,2}}\right\}\cdot\exp\{-4\,(\beta_s-\beta_r)\,f\,z\}, \end{aligned} \tag{4}$$

where the subscripts r and s represent the reference phantom and sample, respectively.

In the spectral difference method, the ratio of the intensities of the echo signals $RS(f,z)$ was used to estimate the attenuation coefficient of the sample by taking the logarithm of the power spectrum and then using linear regression along the depth. However, because the intensities of the echo signals are related to both the local backscatter properties and attenuation properties of the scanned object, the attenuation estimate would be erroneous at the boundaries where the backscatter properties change. This will be illustrated later on with one of our simulations.

In the hybrid method, Gaussian filtering is applied to $RS(f,z)$, centered around the frequency of the transmit pulse, and the downshift of the central frequency as a function of depth was estimated using a spectral shift algorithm. The Gaussian filtered intensity ratio is given by

$$\begin{aligned} GRS(f,z) &= G(f)\cdot RS(f,z) \\ &= \exp\left\{-\frac{(f-f_c)^2}{2\sigma^2}\right\}\cdot\exp\left\{\frac{(n_s-n_r)\cdot(f^2-4f_cf)}{2f_c^{\,2}}\right\} \\ &\quad\cdot\exp\{-4(\beta_s-\beta_r)fz\}, \end{aligned} \tag{5}$$

where $G(f)$ is a Gaussian function at the transmit center frequency, f_c, and has the same variance as the transmit

pulse, σ^2. After manipulating eqn (5) as described in the Appendix, we show that the center frequency of $GRS(f,z)$ at the depth z can be expressed as

$$f_c(z) = \frac{f_c - 4\sigma^2(\beta_s - \beta_r)z + \frac{\sigma^2(n_s - n_r)}{f_c^2}}{1 + \frac{\sigma^2(n_s - n_r)}{f_c^2}}$$

$$\approx f_c - 4\sigma^2(\beta_s - \beta_r)z. \quad (6)$$

Because the transmit center frequency is generally greater than the square root of the variance of the transmit pulse, and the parameter n for human tissue is between 1 and 2, the spectral shift of the center frequency at depth z obtained is linearly proportional to the product of the difference between slope of attenuation coefficients and depth as shown in eqn (6). By differentiating eqn (6) with respect to z, the slope of the spectral shift along depth is proportional to the difference in the slope of attenuation coefficients between the sample and reference phantom. Under the assumption of a linear frequency-dependent attenuation in soft tissue, linear regression over the local spectral shift estimates (usually several blocks along the axial direction) is used to compute the final slope of the attenuation coefficient. The relationship between the slope of downshift of center frequency *vs.* depth and the slope of attenuation coefficient is given by

$$\beta_s\,(dB/cm/MHz) = -\frac{8.686}{4\sigma^2} \cdot \frac{df_c(z)}{dz} + \beta_r, \quad (7)$$

where z is the depth of the ROI from the transducer and σ^2 is the variance of the transmit pulse.

In our hybrid method, a spectral cross-correlation algorithm (Kim and Varghese 2007) was used to estimate the spectral shift. This algorithm was preferred to the simple calculation of the center frequency of the spectrum at each depth, because it provides a more accurate and stable estimate of the spectral shift. Because the attenuation is linearly proportional to the derivative of the center frequency with respect to depth in eqn (7), estimation of the absolute value of the center frequency is not required for the estimation of the slope of the attenuation.

RF data simulation

RF signals for both the reference phantom and the sample phantom were generated using a simulation program (Li and Zagzebski 1999; Chen 2004). This program is based on the classical linear diffraction theory of continuous waves. In this program, the beam pattern of an ultrasound pulse transmitted by a series of sources (such as array elements) is computed using the superposition principle. For this study, a linear array transducer consisting of 128 rectangular elements, 0.2 mm in width (azimuthal direction) by 10 mm in length (elevation direction), with a center-to-center separation of 0.2 mm, was used as transmitter and receiver. Each beam line formed by the array used 128 consecutive elements, and the array field is a superposition of simultaneous excitation of these single elements. On receive, dynamic focusing was used in combination with dynamic aperture such that the F-number on receive was fixed at 2 and independent of depth. A Gaussian-shaped pulse with a center frequency of 5 MHz and a bandwidth of 80% was simulated for the transmit pulse at the surface of the sample. In this simulation software, a complex wave number is used to introduce specific values of the speed-of-sound and attenuation in the medium of propagation.

The reference phantom, which was uniform in backscatter and attenuation properties, was simulated using 25-μm glass beads. The scatterer number density was set to 9.7 per cubic millimeter, and the attenuation slope was set to 0.3 dB/cm/MHz. The speed-of-sound in the medium was assumed to be 1540m/s. To compare the estimation performance quantitatively, five different phantoms containing inclusions with different scattering properties were simulated. The five inclusion phantoms consist of random distribution of 50-μm polystyrene beads and possess backscatter intensity values ranging from 6 dB lower than the background to 6 dB higher than the background, in increments of 3 dB that were obtained by changing the scatterer number density. The attenuation slopes of the inclusion and background were both set to 0.5 dB/cm/MHz.

All numerical phantoms were 40 mm wide, 40 mm deep and 10 mm thick. The distance between simulated beam lines was set to 0.2 mm, resulting in 192 simulated RF lines for each phantom (including computational margins on the left and right sides). The transducer was assumed to be in direct contact with the sample or reference phantom, and the axial transmit focus as well as the elevational focus were both set at 40 mm. Simulations were performed over a 1–15 MHz frequency range, using an increment of 0.1 MHz between frequency components. The backscattered signals were computed by first applying a Gaussian filter centered at 5 MHz with the specified frequency bandwidth of the transducer, and then computing the inverse Fourier transform. This yielded RF echo data for each beam line that was used to form the simulated ultrasound images.

Experimental RF data acquisition

Two tissue-mimicking (TM) phantoms manufactured in our laboratory were also used to test the performance of the hybrid method. The reference phantom was uniform and consisted of 45–53-μm glass beads in a

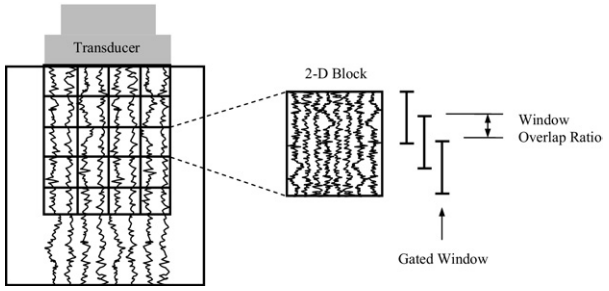

Fig. 1. Schematic diagram illustrating computation of the block power spectrum for attenuation estimation. After acquiring RF echo signal frames, the entire frame (or selected ROI) was subdivided into small 2-D overlapping blocks (the overlapping of the blocks is not shown in this figure). Each block contains several A-lines in the lateral direction. Each A-line in the block is further divided into segments in the axial direction with a 50% overlap, where the segments are gated using a Hanning window. The complex Fourier spectra computed over each of the gated data segments are then time-averaged (to obtain the expected value) to generate the power spectrum.

gelatin for which the attenuation slope was 0.5 dB/cm/MHz (Wilson et al. 2002). The attenuation phantom (AP) consisted of two cylindrical inclusions containing 20-μm glass beads. These inclusions, which had an attenuation slope of 0.8 dB/cm/MHz, were embedded in a medium identical to the reference phantom. One of the inclusions had a scattering coefficient identical to the surrounding medium, whereas the other had a scattering coefficient 3 dB higher than the surrounding medium.

The TM phantoms were scanned using a Siemens Antares ultrasound system (Siemens Medical Systems, Issaquah, WA, USA) using a linear array transducer operated at a 5-MHz center frequency with an 80% bandwidth. The AP was scanned across two different regions that include each cylindrical inclusion. Three ROI were selected, one above, one under and one inside the inclusion, in which the attenuation coefficients were estimated. RF data from each of these regions were acquired at five independent locations along the cylindrical inclusion. In each region, power spectra were calculated at different depths. For each of these depths, the average power spectrum was calculated and used to improve the accuracy of the results.

RF data processing

After acquiring RF data, the RF data frame was divided into smaller overlapping 2-D blocks of sufficient size to obtain a stable power spectrum which contains correct frequency information from RF signals, as illustrated in Fig. 1. The 2-D block size should be small enough to satisfy the stationarity assumption, namely no variation in the attenuation, as well as provide sufficient spatial resolution for the attenuation estimate. However, the block size has to be large enough to generate an accurate and robust power spectrum of the backscattered RF signals. A criteria based on the evaluation of the full-width-half-maximum (FWHM) of the power spectrum (Kim and Varghese 2007) was used to determine the block size that would provide a consistent power spectrum. A complete list of the parameters used to calculate power spectra are indicated in the simulation and experiment result sections. The block power spectrum was calculated using short-time Fourier analysis by averaging spectra from windowed segments within the block (Welch 1967). In each 2-D block, the gated window size was set to half the axial length of the block with a 50% window overlap used to calculate the block power spectrum. Each windowed RF segment was gated by a Hanning window to minimize spectral leakage artifacts. Each block contained 10 beam lines in the lateral direction and each block power spectrum was obtained from an average of 30 Fourier spectra. A 50% overlap of the 2-D blocks was applied along the axial and lateral directions respectively to obtain a map of the slope of attenuation coefficients. Frequency smoothing where adjacent frequency estimates are averaged using a moving average window (Varghese and Donohue 1995), was also utilized to further reduce spectral noise artifacts in the power spectra.

After estimating the block power spectra from the gated echo signals, the spectral difference method was utilized by calculating the ratio of the intensities of echo signals from the sample and reference phantom to eliminate the system and transducer-dependent parameters. Gaussian filtering at the transmit center frequency with the same bandwidth as the transmit pulse was then applied to the ratio of intensities of echo signals, and the

Fig. 2. B-mode and attenuation coefficient images of simulated numerical TM inclusion phantoms. Both the inclusion and the background have the same value of the attenuation coefficient of 0.5 dB/cm/MHz, but different levels of backscatter, where the column denoted by (a) depicts the phantom where the backscatter of the inclusion is 6 dB lower than the background, (b) same backscatter level in the inclusion and background and (c) inclusion with a 6 dB higher backscatter level. B-mode images of the phantoms are shown in the first row (i), attenuation coefficient images using the spectral difference method (reference phantom method) in row (ii), attenuation coefficient images using the spectral shift method (centroid downshift method) in row (iii) and finally the attenuation coefficient images obtained using the hybrid method in row (iv).

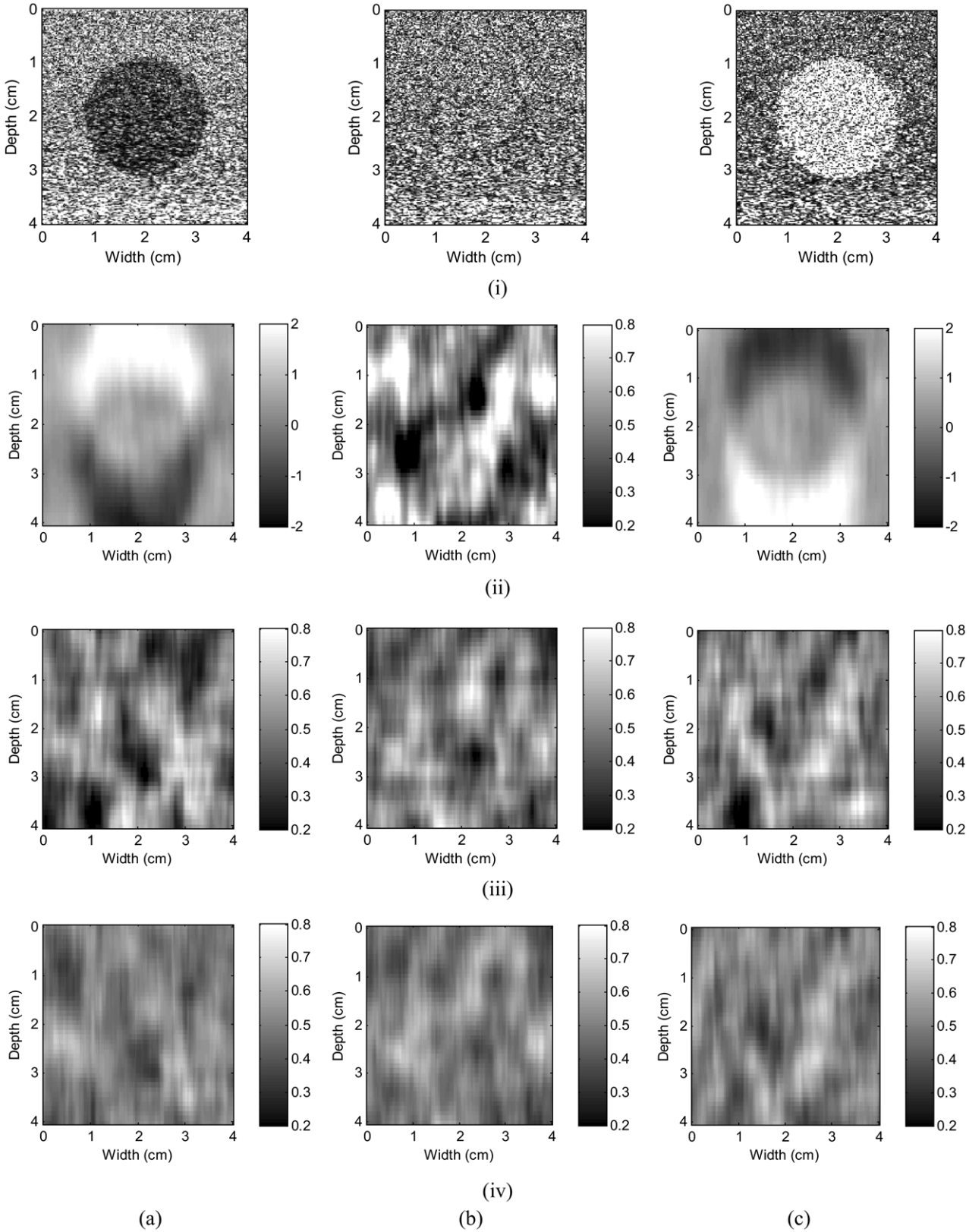
(i)
(ii)
(iii)
(iv)
(a)
(b)
(c)
Depth (cm)
Width (cm)

spectral cross-correlation algorithm was utilized to compute the spectral shift between two consecutive power spectra. The spectral shift was obtained from the location of the maximum of the cross-correlation function. The spectral shift was equivalent to the center frequency downshift obtained from two consecutive centroid estimates. The slope of the attenuation was estimated by calculating the slope of the linear regression of the frequency shift estimates as function of depth.

To compare the hybrid algorithm with other spectral domain methods of estimation of the attenuation slope, simulated and experimental data were also processed using the centroid downshift method (Fink et al. 1983) and the reference phantom method (Yao et al. 1990) as the spectral shift and spectral difference methods respectively. In the centroid downshift method, the spectral shift was estimated by calculating the centroid of the spectrum as a function of depth, from which the attenuation slope was estimated using eqn (7). In the reference phantom method, after compensation of the diffraction and system effects using eqn (4), the attenuation coefficient $\alpha(f)$ was calculated as the slope of the linear regression of $ln(RS(f, z))$ as a function of z at each frequency f, and the attenuation slope was estimated by calculating the slope of linear regression of $\alpha(f)$ as a function of f.

RESULTS AND DISCUSSION

Simulation results

In this section, we compare the estimation performances for three different inclusion cases using all three frequency-domain methods described earlier. The first row of images in Fig. 2, depict the B-mode images (Fig. 2(i)) of the simulated TM phantoms. While the slope of attenuation coefficient of the background and the cylindrical inclusions were the same at 0.5 dB/cm/MHz, the backscatter levels of the inclusion were different when compared to the background by a factor of −6 dB, 0 dB and +6 dB as depicted in Fig. 2a, b and c, respectively. After computing the FWHMs of the power spectra for various block sizes, the 2-D block size for the computation of the power spectra was selected as 4 × 4 mm along the axial and lateral dimensions respectively. The linear fit window was set to 1 cm to obtain attenuation coefficient images.

The second row of images in Fig. 2(ii) present the estimated attenuation coefficient images obtained using the spectral difference method. For the inclusion with the 6 dB lower value of the backscatter, the spectral difference method overestimates the attenuation coefficient at the top of the inclusion and underestimates it at the bottom of the inclusion, where changes in backscatter intensity occur (Fig. 2(ii)(a)). This is due to the relative variation in the intensities of the echo signals due to the backscatter level differences at the boundary of the inclusion. For the inclusion with the 6 dB higher value of the backscatter, on the other hand, the spectral difference method underestimates attenuation coefficients at the start of the backscatter intensity variations and overestimates it at the end of inclusion, as shown in Fig. 2 (ii)(c). Note that the dynamic range of these two images is different from the other attenuation coefficient images since the range of estimated values is larger than the other cases. However, when the inclusion has same backscatter level as the background, as shown in Fig. 2 (ii)(b), no boundary effects are observed for the spectral difference method.

The third and fourth rows of Fig. 2 present the estimated attenuation coefficient images obtained using spectral shift method (Fig. 2(iii)) and the hybrid method (Fig. 2(iv)), respectively. These two methods exhibit no boundary effects due to the backscatter variations and estimate the attenuation coefficient relatively uniformly over the entire images. Although both estimation methods demonstrate fluctuations in the estimation of the attenuation coefficients, the hybrid method overall shows smaller estimation variances when compared to the spectral shift method since the spectral shift method is more sensitive to fluctuations in the shift of the spectral peak due to noise artifacts, and is also more sensitive to the signal-to-noise ratios of the frequency components of the power spectrum.

To compare the estimation performances in a more quantitative fashion, we selected ROIs along the axial direction of the +6 dB inclusion sample, as shown by the dashed rectangle in Fig. 3a. The width of the selected ROI was 1.2 cm. Figure 3b shows plots of the estimated slope of attenuation coefficients *vs.* depth using the three different attenuation estimation methods. As shown in Fig. 2(ii)(c), the spectral difference method underestimates the attenuation coefficient at the top boundary of the inclusion and overestimates it at the bottom boundary along the axial direction. The spectral shift method and hybrid method both provide stable estimates of the attenuation coefficient along the entire ROI. Table 1 shows the estimated slope of attenuation coefficients and their standard deviations estimated in the three different ROIs at different depths as indicated in Fig. 3a. The dimensions of all three ROIs were 0.8 × 0.8 mm, and denoted by A, B, and C in Fig. 3a. Although the spectral shift method and the hybrid methods exhibit similar estimation performances in all three regions, the estimation accuracy and precision of the hybrid method is relatively better than that of the spectral shift method.

In Fig. 4, performances of the different attenuation slope estimators are compared as a function of the backscattering intensity of the inclusion relative to the back-

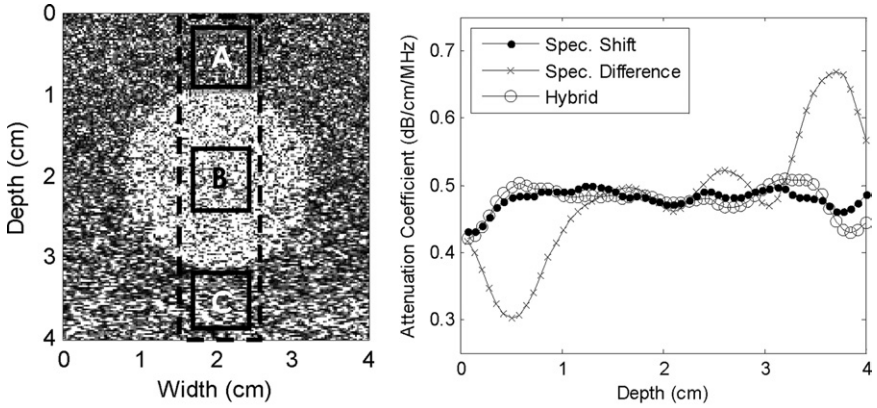

(a) (b)

Fig. 3. Diagram illustrating the (a) regions-of-interest (ROIs) for quantitative comparison of attenuation slope estimation performance for the three different attenuation estimation methods compared. (b) Estimated slope of attenuation coefficients obtained using the simulated TM phantom with the 6 dB higher backscatter level in the inclusion *vs.* depth.

ground. Two ROIs of the same size were selected at positions A and C as shown in Fig. 3a. In region A, the error in the estimate obtained using the spectral difference method increases when the absolute difference in backscattering intensity between inclusion and background increases. The spectral difference method even produces negative attenuation slope values when the difference in backscattering intensity between inclusion and background are larger than the effect of attenuation over small data segments. The estimate obtained using the spectral shift method stays constant over the range of backscatter intensity in the inclusion, which it should, because the attenuation slope value is uniformly the same in these five simulated phantoms. However, it suffers from a systematic bias that is associated with the fact that this estimation method does not compensate for diffraction effects. The hybrid method, however, produces stable estimation results independent of backscatter intensity changes. For the estimation results in region C, they indicate the same trend as that of region A. As the difference between the backscatter intensities between the inclusion and background increase, the estimation errors using the spectral difference methods also become larger.

Experimental results

In addition to the simulation, we also investigate the estimation performance among the three spectral domain algorithms using TM phantoms as described in the previous section. Although the reference TM phantom has a uniform attenuation value of 0.5 dB/cm/MHz, the sample TM phantom has two cylindrical inclusions located in the middle of the background region with an attenuation coefficient value of 0.8 dB/cm/MHz. Note that the inclusion in the left image of Fig. 5 has a 3-dB higher backscatter intensity than the background, whereas the other inclusion has the same backscatter intensity as the background. Figure 5 presents B-mode images of two inclusions. Because the left cylindrical inclusion had a backscatter intensity level that was 3 dB higher than the background, the inclusion appears brighter in Fig. 5a. On the other hand, the inclusion on the right is not clearly visualized in the B-mode image because it has the same backscatter intensity as the background, as shown in Fig. 5b. Three rectangular ROIs, whose locations are shown in Fig. 5, were selected to compare the performances of the hybrid method to those of the two classical spectral domain methods.

Figure 6 shows the estimation results for the three spectral domain methods in the three ROIs indicated in Fig. 5. After evaluating the FWHM values of the power spectra obtained from different block sizes, the 2-D block size for the power spectra was selected to be 6 × 6 mm along the axial and lateral dimensions, respectively. For the left inclusion, whose backscatter intensity

Table 1. Estimated slope of attenuation coefficients and standard deviations (dB/cm/MHz)

	Spectral shift method		Spectral difference method		Hybrid method	
	Mean	STD	Mean	STD	Mean	STD
Region A	0.4844	0.0279	0.3503	0.0187	0.4949	0.0303
Region B	0.4881	0.0336	0.4726	0.0147	0.4867	0.0301
Region C	0.4792	0.0344	0.5786	0.0369	0.4954	0.0319

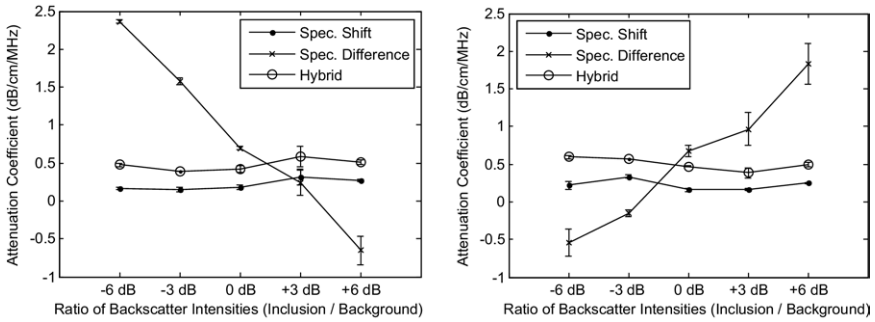

Fig. 4. Estimated slope of the attenuation coefficients for TM inclusions with different backscatter levels for ROIs located above and below the inclusion boundary. The ROIs are selected with the same dimensions at position A and C as shown in Fig. 3a, where the error bars represent the standard deviation of estimated slope of attenuation coefficients. (a) Region A: beginning of inclusion boundary. (b) Region C: end of inclusion boundary.

is 3 dB higher than the background, as shown in Fig. 6a, the spectral difference method underestimates the slope of attenuation coefficient at the beginning of the inclusion (region A), and overestimates the slope of attenuation coefficient at the end of the inclusion (region C). Because linear regression is used to estimate the slope of attenuation coefficients, the overestimated/underestimated values of the attenuation coefficient slope appear before and after the inclusion boundaries. Comparison of the spectral shift method and the hybrid method indicates that the hybrid method provides better estimation results, with respect to both accuracy and precision. For the right inclusion whose backscatter intensity is the same as the background, shown in Fig. 6b, the spectral difference method and the hybrid method estimate the slope of attenuation coefficient values correctly for all the three regions, whereas the spectral shift method underestimates the slope of the attenuation coefficient in region C.

SUMMARY

The ultrasonic attenuation parameter in soft tissue has been used widely to distinguish between benign and malignant tumors and to detect diffuse diseases in many tissue types. However, the presence of shadowing or enhancement artifacts in the conventional B-mode im-

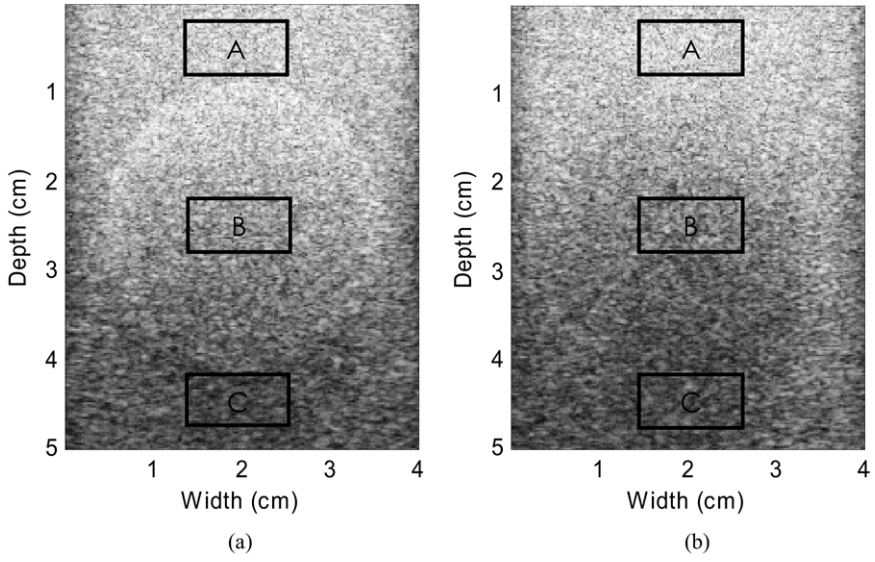

Fig. 5. B-mode images of the tissue-mimicking phantom with a cylindrical inclusion at the center of the uniform background region. The diameter of each cylindrical inclusion was 3 cm and the attenuation coefficient was 0.8 dB/cm/MHz. The attenuation coefficient of the background was 0.5 dB/cm/MHz. (a) The backscatter intensity of the first inclusion is 3 dB higher than that of the background. (b) The backscatter intensity of the second inclusion is the same as that of the background.

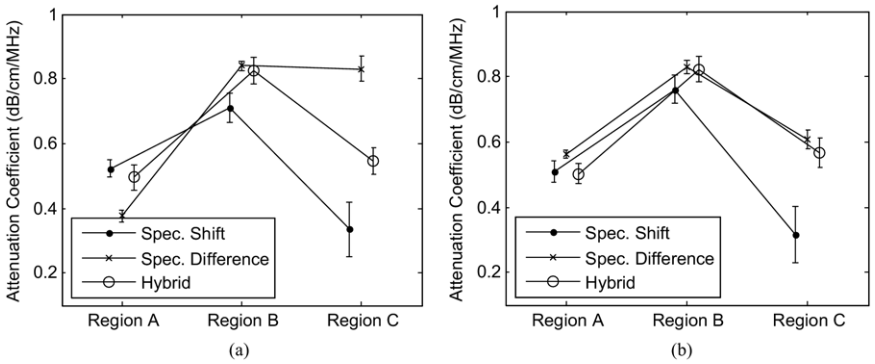

Fig. 6. Estimated slope of attenuation coefficients for the three ROIs shown in Fig. 5. Error bars represent the standard deviation of estimated slope of attenuation coefficients in each ROI. (a) The backscatter intensity of the inclusion is 3 dB higher than that of the background. (b) The backscatter intensity of the inclusion is the same as that of the background.

ages makes interpretation of the B-mode images more difficult. Therefore, accurate estimation of ultrasonic attenuation would not only provide useful diagnostic information, but also enable clear interpretation of the B-mode images for further analysis.

The classical spectral shift and spectral difference methods for the estimation of attenuation have limitations, respectively, an inability to compensate for diffraction effects and a sensitivity to backscatter intensity variations. In this paper, we propose a new hybrid attenuation estimation method in the frequency domain that incorporates the advantages of both the spectral difference and spectral shift based algorithms. Because the proposed hybrid method also uses a similar approach as other classical frequency domain methods, the diagnostic resolution of the final attenuation images are limited by the block size required to compute stable power spectrum and the size of the linear fit window. However, because we precompute the optimal gated window size using FWHM values of power spectra, it can be used effectively to estimate the attenuation coefficient for all ROIs regardless of backscatter intensity variations. For *in vivo* applications, the hybrid method would require scanning of a reference phantom with identical transducer and system settings as that used to scan the patient, similar to the protocol followed for the reference phantom method. In addition, we would calculate both power spectra using the same block size to obtain normalized power spectra at the same resolution. However, because some of the acoustic parameters between the reference phantom and patient including speed-of-sound and attenuation may be different, these differences may impact the estimation accuracy (Tu and Zagzebski 2006). We therefore have to use appropriate reference phantoms that have similar characteristics as the tissue type being imaged to improve the estimation accuracy and precision.

Ultrasound simulation results demonstrate that the estimation accuracy of the hybrid method is better than the centroid downshift method (spectral shift method), for uniform attenuation regions. In addition, it is also stable at boundaries with variations in the backscatter when compared with the reference phantom method (spectral difference method). Experimental results using TM phantoms also illustrate that the hybrid method is more robust and provides accurate attenuation estimates in both uniformly attenuating regions and regions with backscatter variations. The proposed hybrid method preserves the advantages of both the spectral shift and spectral difference approaches while eliminating the disadvantages of both of these methods, thereby improving estimation accuracy and robustness of attenuation estimation.

Acknowledgements—The authors acknowledge the efforts of the reviewers for their helpful comments and constructive suggestions for this paper. Their efforts have helped significantly in improving this paper.

REFERENCES

Baldeweck T, Laugier P, Herment A, Berger G. Application of autoregressive spectral analysis for ultrasound attenuation estimation: Interest in highly attenuating medium. IEEE Trans Ultrason Ferroelectr Freq Control 1995;42:99–109.

Baldwin SL, Holland MR, Sosnovik DE, Miller JG. Effects of region-of-interest length on estimates of myocardial ultrasonic attenuation and backscatter. Med Phys 2005;32(2):418–426.

Baldwin SL, Marutyan KR, Yang M, Wallace KD, Holland MR, Miller JG. Measurements of the anisotropy of ultrasonic attenuation in freshly excised myocardium. J Acoust Soc Am 2006;119(5 Pt 1):3130–3139.

Berger G, Laugier P, Thalabard JC, Perrin J. Global breast attenuation: Control group and benign breast diseases. Ultrason Imaging 1990; 12:47–57.

Bigelow TA, Oelze ML, O'Brien WD Jr. Estimation of total attenuation and scatter size from backscattered ultrasound waveforms. J Acoust Soc Am 2005;117(3):1431–1439.
Bridal SL, Fournier C, Coron A, Leguerney I, Laugier P. Ultrasonic backscatter and attenuation (11–27 MHz) variation with collagen fiber distribution in ex vivo human dermis. Ultrason Imaging 2006; 28(1):23–40.
Chen Q. Computer simulations in parametric ultrasonic imaging (PhD dissertation), University of Wisconsin-Madison, 2004.
Fink M, Hottier F, Cardoso JF. Ultrasonic signal processing for in vivo attenuation measurement: Short time Fourier analysis. Ultrason Imaging 1983;5:117–135.
Flax SW, Pelc NJ, Glover GH, Gutmann FD, McLachlan M. Spectral characterization and attenuation measurements in ultrasound. Ultrason Imaging 1983;5:95–116.
Fujii Y, Taniguchi N, Itoh K, Shigeta K, Wang Y, Tsao JW, Kumasaki K, Itoh T.. A new method for attenuation coefficient measurement in the liver: Comparison with the spectral shift central frequency method. J Ultrasound Med 2002;21(7):783–788.
Hall TJ, Insana MF, Harrison LA, Cox GG. Ultrasonic measurement of glomerular diameters in normal adult humans. Ultrasound Med Biol 1996;22(8):987–997.
He P, Greenleaf JF. Attenuation estimation on phantoms—A stability test. Ultrason Imaging 1986;8:1–10.
Huang SW, Li PC. Ultrasonic computed tomography reconstruction of the attenuation coefficient using a linear array. IEEE Trans Ultrason Ferroelectr Freq Control 2005;52(11):2011–22.
Insana MF, Wagner RF. Describing small-scale structure in random media using pulse-echo ultrasound. J Acoust Soc Am 1990;87: 179–192.
Jang HS, Song TK, Park SB. Ultrasound attenuation estimation in soft tissue using the entropy difference of pulsed echoes between two adjacent envelope segments. Ultrason Imaging 1988;10:248–264.
Kasai C, Namekawa K, Koyano A, Omoto R. Real-time two-dimensional blood flow imaging using an autocorrelation technique. IEEE Trans Sonic Ultrason 1985;32:458–464.
Kim H, Varghese T. Attenuation estimation using spectral cross-correlation. IEEE Trans Ultrason Ferroelectr Freq Control 2007;54: 510–519.
Knipp BS, Zagzebski JA, Wilson TA, Dong F, Madsen EL. Attenuation and backscatter estimation using video signal analysis applied to B-mode images. Ultrason Imaging 1997;19:221–233.
Kuc R. Bounds on estimating the acoustic attenuation of small tissue regions from reflected ultrasound. Proc IEEE 1985;73:1159–1168.
Kuc R, Li H. Reduced-order autoregressive modeling for center-frequency estimation. Ultrason Imaging 1985;7:244–251.
Levy Y, Agnon Y, Azhari H. Measurement of speed of sound dispersion in soft tissues using a double frequency continuous wave method. Ultrasound Med Biol 2006;32(7):1065–1071.
Li Y, Zagzebski JA. A frequency domain model for generating B-mode images with array transducers. IEEE Trans Ultrason Ferroelectr Freq Control 1999;46:690–699.
Liu W, Zagzebski JA, Varghese T, Gerig AL, Hall TJ. Spectral and scatterer-size correlation during angular compounding: Simulations and experimental studies. Ultrason Imaging 2006;28(4):230–244.
Meziri M, Pereira WC, Abdelwahab A, Degott C, Laugier P. In vitro chronic hepatic disease characterization with a multiparametric ultrasonic approach. Ultrasonics 2005;43(5):305–313.
Narayana PA, Ophir J. On the frequency dependence of attenuation in normal and fatty liver. IEEE Trans Sonics Ultrason 1983;30:379–383.
Ophir J, McWhirt RE, Maklad NF, Jaeger PM. A narrowband pulse-echo technique for in vivo ultrasonic attenuation estimation. IEEE Trans Biomed Eng 1985;32:205–212.
Robinson DE, Ophir JO, Wilson LS, Chen CF. Pulse-echo ultrasound speed measurements: Progress and prospects. Ultrasound Med Biol 1991;17:633–646.
Taggart LR, Baddour RE, Giles A, Czarnota GJ, Kolios MC. Ultrasonic characterization of whole cells and isolated nuclei. Ultrasound Med Biol 2007;33(3):389–401.
Techavipoo U, Varghese T, Chen Q, Stiles TA, Zagzebski JA, Frank GR. Temperature dependence of ultrasonic propagation speed and attenuation in excised canine liver tissue measured using transmitted and reflected pulses. J Acoust Soc Am 2004;115(6): 2859–2865.
Towa RT, Miller RJ, Frizzell LA, Zachary JF, O'Brien WD Jr. Attenuation coefficient and propagation speed estimates of rat and pig intercostal tissue as a function of temperature. IEEE Trans Ultrason Ferroelectr Freq Control 2002;49(10):1411–1420.
Treece G, Prager R, Gee A. Ultrasound attenuation measurement in the presence of scatter variation for reduction of shadowing and enhancement. IEEE Trans Ultrason Ferroelectr Freq Control 2005;52: 2346–2360.
Tu H, Zagzebski JA, Chen Q. Attenuation estimations using envelope echo data: Analysis and simulations. Ultrasound Med Biol 2006: 32:3:377–386.
Varghese T, Donohue KD. Estimating mean scatterer spacing with the frequency-smoothed spectral autocorrelation function. IEEE Trans Ultrason Ferroelectr Freq Control 1995;42:451–463.
Vered Z, Mohr GA, Barzilai B, Gessler CJ, Wickline SA, Wear KA, Shoup TA, Weiss AN, Sobel BE, Miller JG. Ultrasound integrated backscatter tissue characterization of remote myocardial infarction in human subjects. J Am Coll Cardiol 1989;13:84–91.
Wear KA. Ultrasonic attenuation in human calcaneus from 02 to 17 MHz. IEEE Trans Ultrason Ferroelectr Freq Control 2001;48:602–608.
Wear KA. Characterization of trabecular bone using the backscattered spectral centroid shift. IEEE Trans Ultrason Ferroelectr Freq Control 2003;50(4):402–407.
Wear KA, Garra BS, Hall TJ. Measurements of ultrasonic backscatter coefficients in human liver and kidney in vivo. J Acoust Soc Am 1995;98:1852–1857.
Wear KA, Stiles TA, Frank GR, Madsen EL, Cheng F, Feleppa EJ, Hall CS, Kim BS, Lee P, O'Brien WD Jr., Oelze ML, Raju BI, Shung KK, Wilson TA, Yuan JR. Interlaboratory comparison of ultrasonic backscatter coefficient measurements from 2 to 9 MHz. J Ultrasound Med 2005;24(9):1235–1250.
Welch P. The use of fast Fourier transform for the estimation of power spectra: A method based on time averaging over short, modified periodograms. IEEE Trans Audio Electroacoust 1967;15:70–73.
Wilson T, Zagzebski JA, Li Y. A test phantom for estimating changes in the effective frequency of an ultrasonic scanner. J Ultrasound Med 2002;21:937–945.
Yao LX, Zagzebski JA, Madsen EL. Backscatter coefficient measurements using a reference phantom to extract depth-dependent instrumentation factors. Ultrason Imaging 1990;12:58–70.
Zagzebski JA, Lu ZF, Yao LX. Quantitative ultrasound imaging: In vivo results in normal liver. Ultrason Imaging 1993;15:335–351.
Zhao B, Basir OA, Mittal GS. Estimation of ultrasound attenuation and dispersion using short time Fourier transform. Ultrasonics 2004;43: 375–381.

APPENDIX

The Gaussian filtered intensity ratio, shown in eqn (5), can be written as

$$GRS(f,z) = G(f)\cdot RS(f,z)$$
$$= \exp\left\{-\frac{(f-f_c)^2}{2\sigma^2}\right\}\cdot\exp\left\{-\frac{(n_s-n_r)\cdot(f^2-4f_cf)}{2f_c^2}\right\}$$
$$\cdot\exp\left\{-4\,(\beta_s-\beta_r)\,f\,z\right\}, \quad \text{(A1)}$$

where f_c and σ^2 denote the center frequency and variance of the transmit pulse, respectively. The backscatter properties of a reference phantom and sample are represented by n_r and n_s, respectively. Because all terms in eqn (A1) are represented in exponential form, we can simplify it and obtain

$$GRS(f,z) = \exp\left\{-\frac{A}{2\sigma^2f_c^2}\right\}, \quad \text{(A2)}$$

where

$$A = (f-f_c)^2f_c^2 + \sigma^2(n_s-n_r)\cdot(f^2-4f_cf) + 8\sigma^2f_c^2(\beta_s-\beta_r)\,f\,z. \quad \text{(A3)}$$

To estimate the shifted center frequency of the Gaussian filtered intensity ratio, $GRS(f,z)$ eqn (A3) can be rewritten as

$$A = B \cdot \left(f - \frac{C}{B} \right)^2 - \frac{C^2}{B} + f_c^4, \tag{A4}$$

where

$$B = f_c + \sigma^2 \left(n_s - n_r \right), \tag{A5}$$

$$C = f_c \left(f_c^2 + 2\sigma^2 \left(n_s - n_r \right) - 4\sigma^2 f_c \left(\beta_s - \beta_r \right) z \right). \tag{A6}$$

The shifted center frequency at depth z, $f_c(z)$, can be written as

$$f_c(z) = \frac{C}{B} = \frac{f_c - 4\sigma^2(\beta_s - \beta_r)z + \dfrac{\sigma^2(n_s - n_r)}{f_c^2}}{1 + \dfrac{\sigma^2(n_s - n_r)}{f_c^2}},$$

$$\approx f_c - 4\sigma^2(\beta_s - \beta_r)z. \tag{A7}$$

Because the center frequency is generally greater than the square root of the variance of the transmit pulse and the parameter n for human tissue is between 1 and 2 (Wear et al. 1995), the spectral shift of the center frequency obtained is linearly proportional to the product of the difference of the slope of attenuation coefficients and to the depth as shown in eqn (A7).